Progress in Nuclear Energy 51 (2009) 624–636

Contents lists available at ScienceDirect

Progress in Nuclear Energy

journal homepage: www.elsevier.com/locate/pnucene

Analysis on the neutron kinetics for a molten salt reactor

D.L. Zhang [a,b], S.Z. Qiu [a,b,*], G.H. Su [a,b], C.L. Liu [b], L.B. Qian [b]

[a] State Key Laboratory of Multi Phase Flow in Power Engineering, Xi'an Jiaotong University, Xi'an, Shaanxi 710049, PR China
[b] Department of Nuclear and Thermal Power Engineering, Xi'an Jiaotong University, Xi'an, Shaanxi 710049, PR China

Keywords:
Molten salt reactor
Neutron kinetics
Rods drop
Pump coastdown
Inlet temperature drop

A B S T R A C T

The neutron kinetics of the molten salt reactor is significantly influenced by the fuel salt flow, which leads to the analysis methods for the conventional reactors using solid fuels not being applicable for the molten salt reactors. In this study, a neutron kinetic model considering the fuel salt flow is established based on the neutron diffusion theory, which consists of two-group neutron diffusion equations for the fast and thermal neutron fluxes and six-group balance equations for delayed neutron precursors. The temperature feedback on the neutron kinetics is considered by introducing a heat transfer model in the core, in which the group constants which are dependent on the temperature are calculated by the code DRAGON. The mathematical equations are discretized and numerically calculated by developing a code, in which the fully implicit scheme is adopted for the time-dependent terms, and the power law scheme is for the convection–diffusion terms. The neutron kinetics is conducted during three transient conditions including the rods drop transient, the pump coastdown transient and the inlet temperature drop transient. The relative power changes and the distributions of the temperature, neutron fluxes and delayed neutron precursors under these three different transient conditions are obtained in the study. The results provide some valuable information for the research and design of this new generation reactor.

1. Introduction

The advantages of the molten salt reactor (MSR) such as the neutron economy, inherent safety and on-line refueling make the MSR attractive for the present Generation IV International Forum (GIF), and be one of the six candidates for the Generation IV reactors. Therefore, worldwide research activities are being conducted to study and develop new concept molten salt reactors. In Japan, a small molten salt reactor (SMSR) was proposed for utilization of thorium and plutonium from light water reactors (Mitachi et al., 1995). In Russia, a new molten salt reactor concept, molten salt advanced reactor transmutor (MOSART), has been developed for burning plutonium and minor actinides (Ignatiev et al., 2003). In close cooperation with the MOSART project, the MSR technology has been evaluated in the frame of the EU program MOST (MOST PROJECT, 2004).

The neutron kinetics of the molten salt reactors is quite different from that of the conventional reactors using solid fuels due to strong influences of the fuel salt flow. Lapenta et al. (2000) analyzed a transient following a reactivity oscillation for fluid fuel systems by means of the point kinetic model, the conclusion of which shows that the point model is not insufficient when very large perturbations need to be accounted for. Dulla et al. (2003) used the quasi-static method to simulate a velocity step-increased condition in a molten salt reactor similar to MSRE, the calculation workload of which is too tremendous, although the calculation accuracy is a little higher. Yamamoto et al. (2006) performed the transient research during a blockage accident of the SMSR using the neutron diffusion theory. Krepel et al. developed the DYN1D-MSR (Krepel et al., 2005) and DYN3D-MSR (Krepel et al., 2007) codes for the graphite-moderated channel type MSRs, in which some typical transients were conducted such as the reactivity insertion and fuel pump trip.

Although some studies on the molten salt reactors have been carried out by several authors, the molten salt reactors and the objectives they focused on are usually different. In order to provide more basic understanding of the neutron kinetic characteristics of the molten salt reactor, in the present study, three transient conditions including the rods drop transient, pump coastdown transient and the inlet temperature drop transient for the molten salt reactor are simulated by establishing the theoretical model and

* Corresponding author. State Key Laboratory of Multi Phase Flow in Power Engineering, Xi'an Jiaotong University, Xi'an, Shaanxi 710049, PR China
E-mail address: szqiu@mail.xjtu.edu.cn (S.Z. Qiu).

0149-1970/$ – see front matter © 2008 Elsevier Ltd. All rights reserved.
doi:10.1016/j.pnucene.2008.11.008

Nomenclature

C	delayed neutron precursors
G	total groups of the neutron fluxes
I	total families of the delayed neutron precursors
T	temperature
v	velocity of the neutron
U	velocity of the fuel salt
S_T	inner heat source in Eqs. (6) and (7)
E_f	energy released from each fission reaction
K	thermal conductivity
k_{eff}	effective multiplication factor
Cp	specific heat
D	neutron diffusion coefficient

Greek symbols

ρ	density of the fuel salt
ϕ	neutron flux
Σ_r	macroscopic removal cross section
χ_p	fission spectrum of prompt neutron
χ_d	fission spectrum of delay neutron
λ	neutron precursor decay constant
β	delayed neutron fraction
ν	average number of neutrons emitted per fission
Σ_f	macroscopic fission cross section
$\Sigma_{g'-g}$	macroscopic transfer cross section
τ_{loop}	circulate time of the fuel salt in the external loop

Subscripts

g	the neutron flux of group g
i	the delayed neutron precursor of family i
f	fuel salt
c	graphite
in	inlet
out	outlet

developing a code to analyze the neutron kinetic characteristics of the molten salt reactor, in which the temperature feedback to the neutron kinetics is also considered by means of introducing a heat transfer model. The group constants dependent on the temperature are calculated by the code DRAGON. The distributions of the neutron fluxes, the delayed neutron precursors and temperature under the steady state condition and under the transient conditions of rods drop, pump coastdown, and inlet temperature drop are obtained; and the relative power varying with time under these three transient conditions are analyzed.

2. System description

The systematic diagram of the MSR is shown in Fig. 1. Compared with the molten salt reactor experiment and molten salt breeder reactor, the reactor body researched in the present work does not contain graphite or other structure elements in the core. In the primary loop, a ternary molten salt system of 15% LiF–58% NaF–27% BeF_2 functioning as the fuel solvent, coolant and moderator simultaneously works around 873 K at the core inlet. In the present research, 1.0 mol% UF_4 was assumed to be dissolving in this molten salt system as the fuel. The high temperature fuel salt transfers nuclear heat to the secondary molten salt $NaBF_4$–NaF in the primary heat exchanger. The heat is then transferred to helium in the third loop for electricity generation or hydrogen production.

To establish the theoretical model and develop the code, the geometrical configuration of the core was simplified as shown in Fig. 2, in which an (r–z) cylindrical coordinate is used. The core is 380 cm in height and 220 cm in radius, which consists of the fuel salt region and graphite region in thickness of 50 cm.

3. Theoretical model

3.1. Governing equations

Firstly, the multi-group diffusion theory is adopted to establish the neutron kinetic model for the molten salt reactor, which has been validated acceptable in the references Yamamoto et al. (2006), Krepel et al. (2007) and Nicolino et al. (2008). The neutron kinetic model consists of neutron diffusion equations for neutron fluxes and balance equations for delayed neutron precursors. The molten salt reactor is a type of liquid-fuel reactor, in which the delayed neutron precursors drift with the fuel salt flow, which makes the neutron kinetic characteristics of the molten salt reactor different

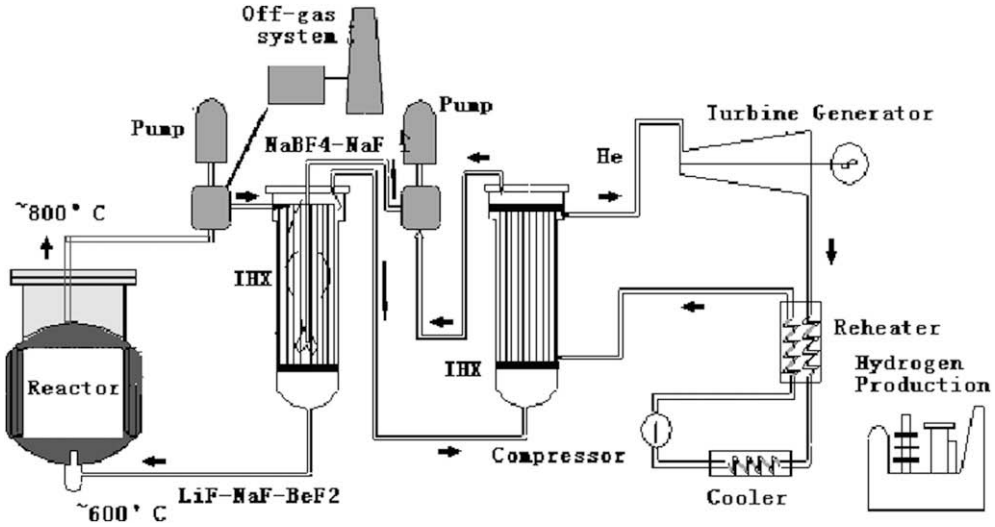

Fig. 1. Schematic diagram of the molten salt reactor system.

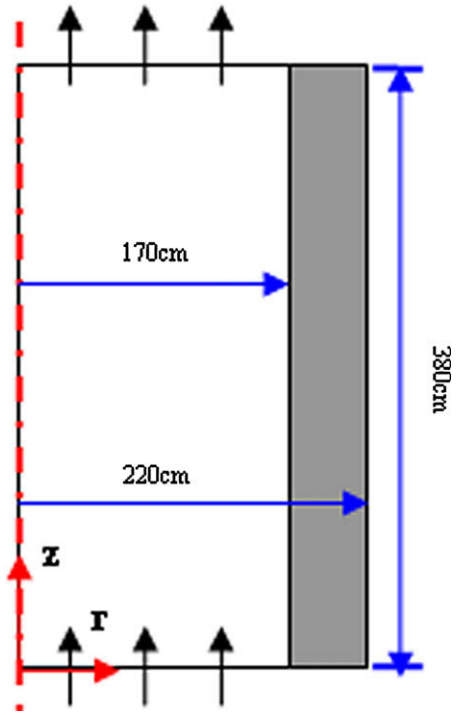

Fig. 2. Geometrical configuration of the reactor core.

from the conventional solid-fuel reactors. Therefore, the flow effect of the fuel salt must be considered when the MSR neutron kinetic model is established.

Classifying the neutron into G groups and the delayed neutron precursors into I families, the diffusion equation for the neutron of group g is derived in a control volume based on the conservation law, which is shown as follows:

$$\frac{1}{v_g}\cdot\frac{\partial\phi_g}{\partial t}+\frac{1}{v_g}\nabla\cdot\left(U\phi_g\right)=\nabla\cdot\left(D_g\nabla\phi_g\right)+\chi_{p,g}\cdot(1-\beta)\cdot\sum_{g=1}^{G}\left(\nu\Sigma_f\right)_g\cdot\phi_g+\sum_{i=1}^{I}\chi_{d,g,i}\cdot\lambda_i\cdot C_i+\sum_{g'=1}^{g-1}\phi_{g'}\cdot\Sigma_{g'\to g}-\phi_g\cdot\Sigma_{r,g} \quad (1)$$

The balance equation for the delayed neutron precursor of family i deduced by the same method is written as

$$\frac{\partial C_i}{\partial t}+\nabla\cdot(UC_i)=\beta_i\cdot\sum_{g=1}^{G}\cdot\left(\nu\Sigma_f\right)_g\cdot\phi_g-\lambda_i\cdot C_i \quad (2)$$

where ϕ: the neutron flux, $cm^{-2}\ s^{-1}$; C: the delayed neutron precursor, cm^{-3}; D: the diffusion coefficient, cm; Σ_f: the macroscopic fission cross section, cm^{-1}; $\Sigma_{g'\to g}$: the macroscopic transfer cross section from the neutron of group g' to group g, cm^{-1}; Σ_r: the macroscopic remove cross section, cm^{-1}; ν: the average number of neutrons emitted per fission; χ_p: the fission spectrum of the prompt neutron; χ_d: the fission spectrum of the delayed neutron; λ_i: the decay constant of the delayed neutron precursor of family i,

Table 1
Delayed neutron fraction and the precursor decay constants.

Group	1	2	3	4	5	6
λ/s^{-1}	0.0124	0.0305	0.111	0.301	1.14	3.01
$\beta/10^{-5}$	22.3	145.7	130.7	262.8	76.6	28.0

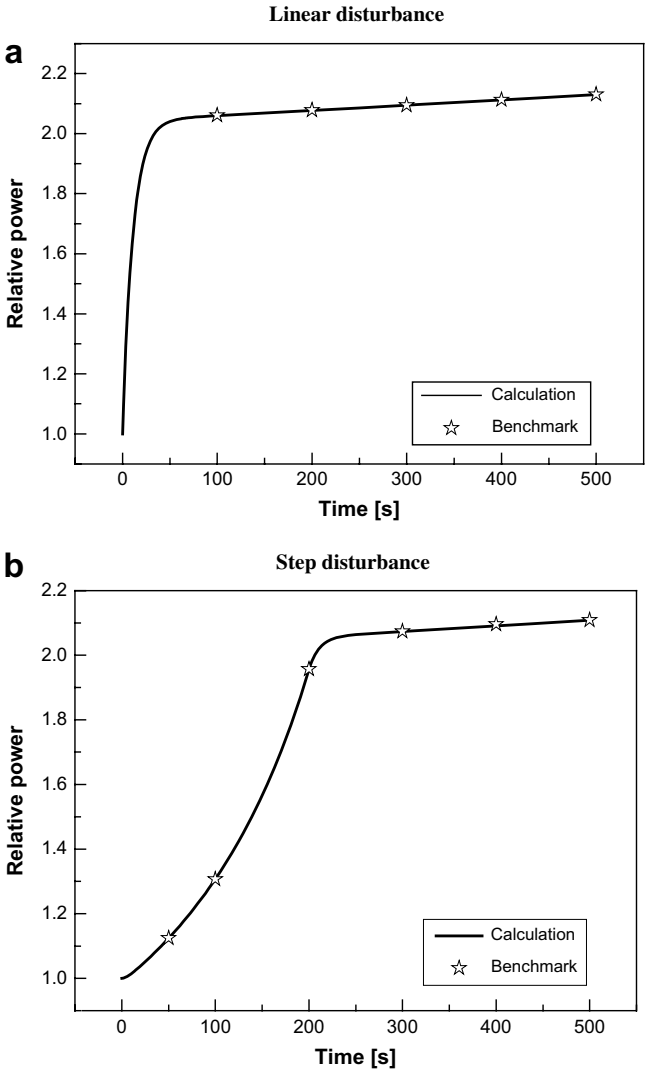

Fig. 3. Transient conditions of the benchmark TWIGL seed blanket.

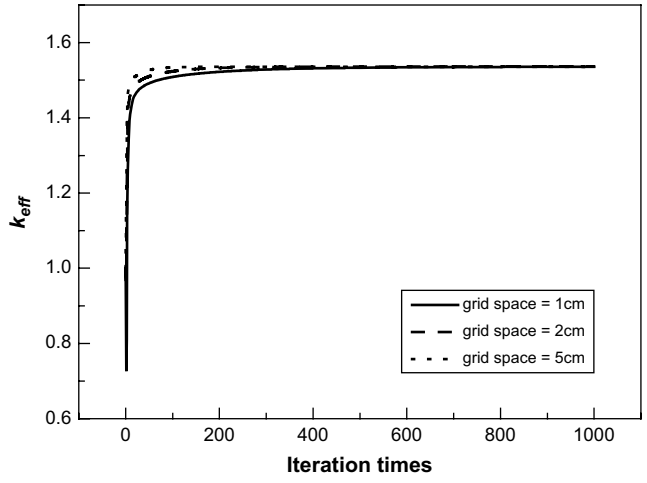

Fig. 4. Sensitivity analysis of the grid dependence.

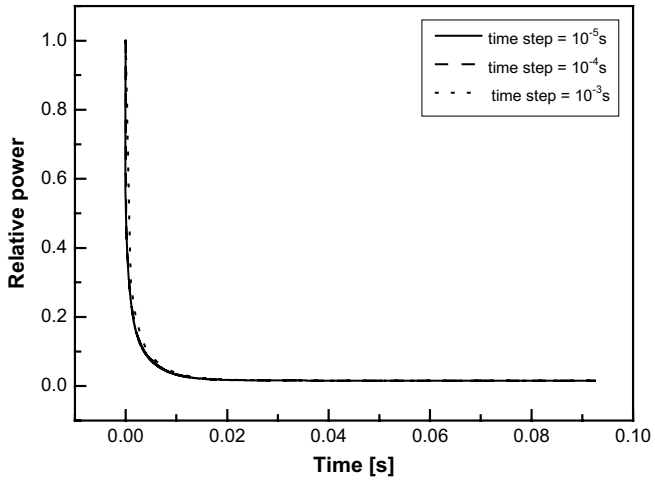

Fig. 5. Sensitivity analysis of the time step dependence.

s^{-1}; β_i: the fraction of the delayed neutron precursor of family i; β: the sum of all β_i, namely $\beta = \sum_{i=1}^{I} \beta_i$; v: the neutron velocity, cm s^{-1}; U: the fuel salt velocity, cm s^{-1}.

The second items in Eqs. (1) and (2) including U are convection items reflecting the flow effect of the fuel salt on the neutron fluxes and precursors, which makes the neutron kinetic model of the molten salt reactor different from those of the conventional reactors using solid fuels.

In the present research, the neutron is classified into two groups, the fast and thermal neutron fluxes marked by the subscripts 1 and 2 respectively, and the delayed neutron precursors are classified into six families by half-life periods. The neutron fission spectrums of prompt neutrons and delayed neutrons are assumed as $\chi_{p,1} = 1$, $\chi_{p,2} = 0$, $\chi_{d,1,i} = 1$, and $\chi_{d,2,i} = 0$ (i = 1–6). Thus the two-group

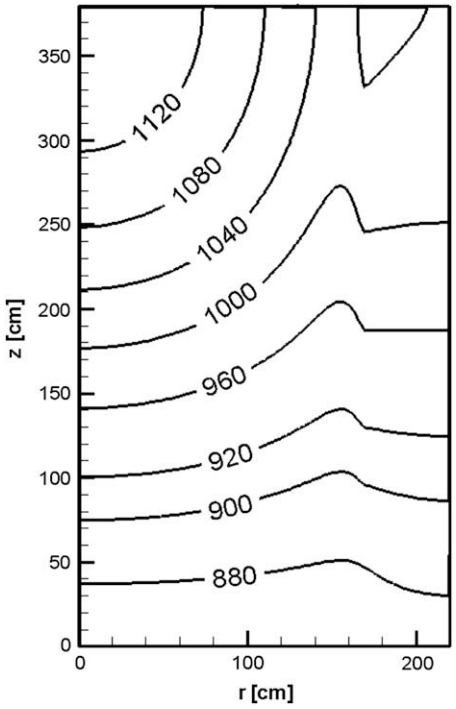

Fig. 6. The temperature distribution under the steady state condition.

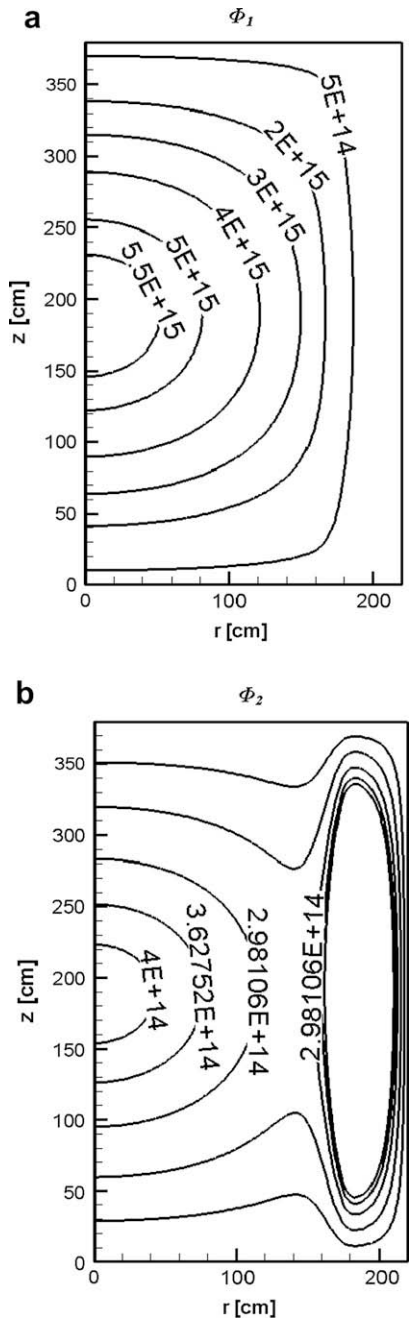

Fig. 7. Distributions of the neutron fluxes under the steady state condition.

neutron diffusion equations for the fast and thermal neutron fluxes are simplified as follows.

$$\frac{1}{v_1}\cdot\frac{\partial \phi_1}{\partial t} + \frac{1}{v_1}\nabla\cdot(U\phi_1) = \nabla\cdot D_1\nabla\phi_1 + (1-\beta)\cdot\sum_{g=1}^{2}\left(\nu\Sigma_f\right)_g\cdot\phi_g + \sum_{i=1}^{6}\lambda_i\cdot C_i - \phi_1\cdot\Sigma_{r,1} \quad (3)$$

$$\frac{1}{v_2}\cdot\frac{\partial \phi_2}{\partial t} + \frac{1}{v_2}\nabla\cdot(U\phi_2) = \nabla\cdot D_2\nabla\phi_2 + \phi_1\Sigma_{1\to 2} - \phi_2\cdot\Sigma_{r,2} \quad (4)$$

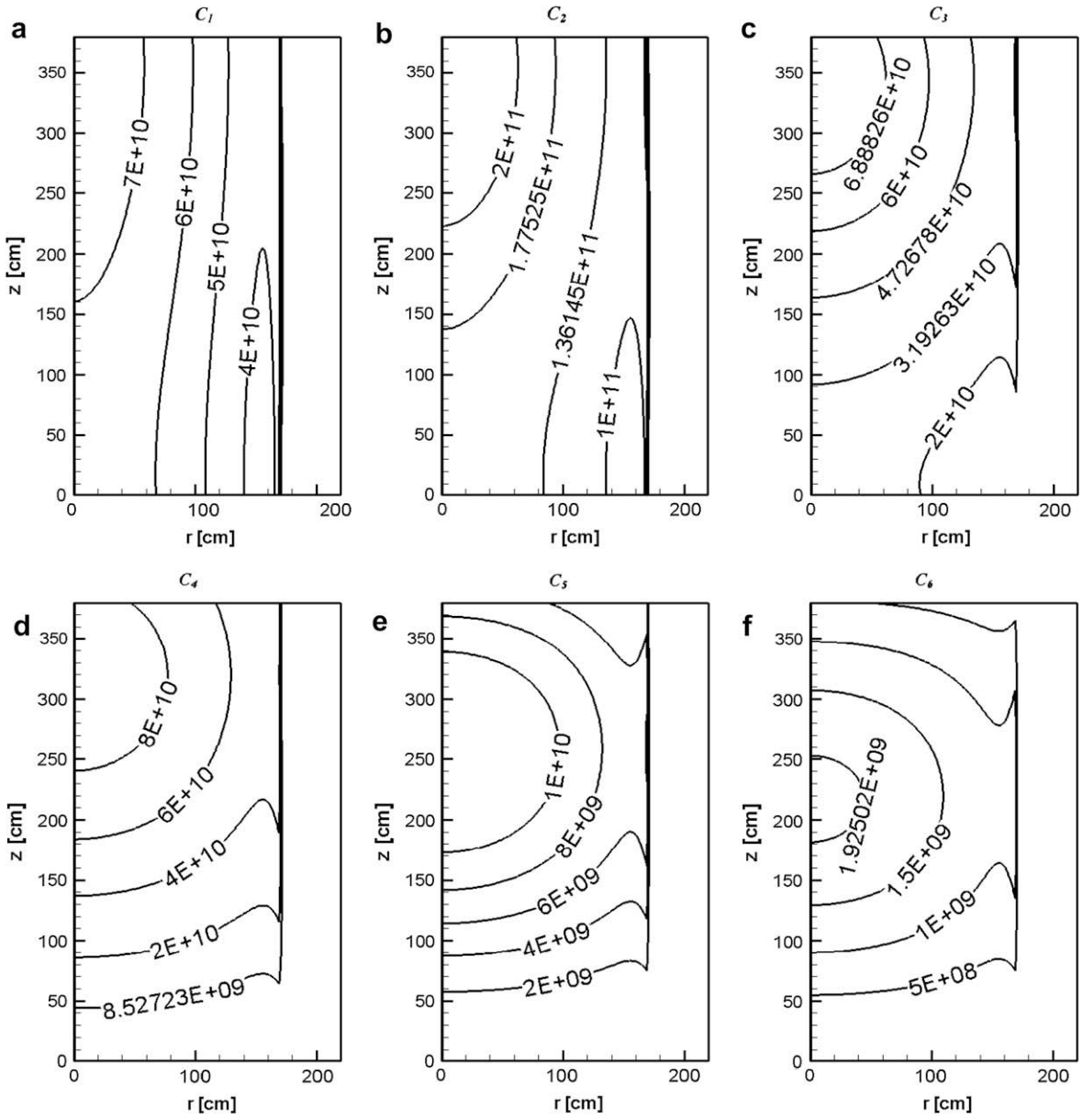

Fig. 8. Distributions of the delayed neutron precursors under the steady state condition.

The balance equation for the delayed neutron precursor of family i is shown in Eq. (5), and the detailed data of β_i and λ_i ($i = 1$–6) are listed in Table 1.

$$\frac{\partial C_i}{\partial t} + \nabla \cdot (UC_i) = \beta_i \cdot \sum_{g=1}^{2} \left(\nu\Sigma_f\right)_g \cdot \phi_g - \lambda_i \cdot C_i \tag{5}$$

Heat transfer in the fuel salt and the graphite is described by energy conservation equations, which are shown in Eqs. (6) and (7).

Table 2
Group constants in the rods region during the rods drop transient.

Parameters	D_1	D_2	$\Sigma_{r,1}/10^{-3}$	$\Sigma_{r,2}/10^{-3}$	$\Sigma_{r,1-2}/10^{-3}$	$(\nu\Sigma_f)_1/10^{-3}$	$(\nu\Sigma_f)_2/10^{-2}$
Values	0.881992	0.077371	52.761853	4104.067	0.000991	0	0

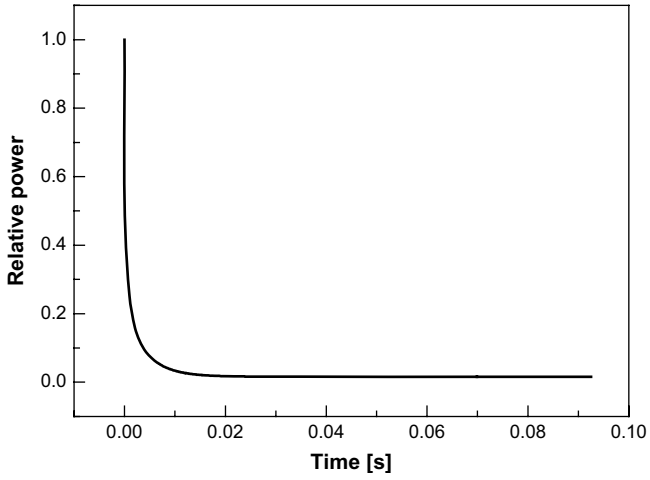

Fig. 9. Behavior of the relative power under the rods drop condition.

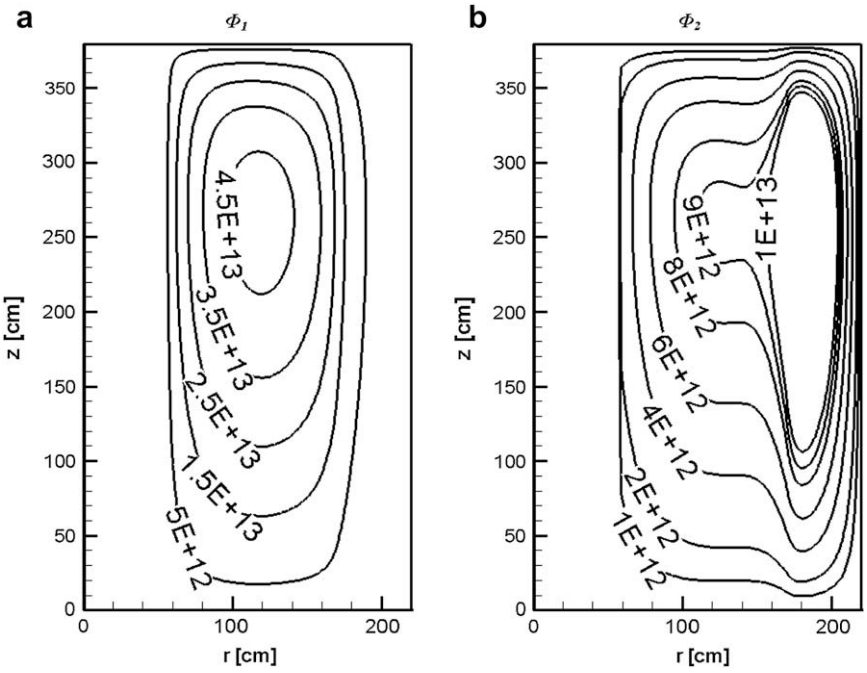

Fig. 10. Distributions of the neutron fluxes after the rods drop 0.05 s.

$$\frac{\partial \rho_f T_f}{\partial t} + \nabla \cdot \left(\rho_f U T_f\right) = \nabla \cdot \frac{K_f}{Cp_f} \nabla T_f + \frac{S_{T,f}}{Cp_f} \tag{6}$$

$$\frac{\partial \rho_c T_c}{\partial t} = \nabla \cdot \frac{K_c}{Cp_c} \nabla T_c + \frac{S_{T,c}}{Cp_c} \tag{7}$$

where ρ_f: the density of the fuel salt, g cm^{-3}; ρ_c: the density of the graphite, g cm^{-3}; Cp_f: the heat capacity of the fuel salt, J g^{-1} K^{-1}; Cp_c: the heat capacity of the fuel salt, J g^{-1} K^{-1}; T_f: the temperature of the fuel salt, K; T_c: the temperature of the graphite reflector, K; K_f: the heat conductivity of the fuel salt, W cm^{-1} K^{-1}; K_c: the heat conductivity of the graphite, W cm^{-1} K^{-1}; $S_{T,f}$: the heat source in the fuel salt, W cm^{-3}; $S_{T,c}$: the heat source in the graphite reflector, W cm^{-3}.

The inner heat sources of the fuel salt and the graphite in Eqs. (6) and (7) can be calculated from the neutron fission reactions. The 90% fission energy is the kinetic energy of fission fragments released into the fuel salt (Yamamoto et al., 2006). The remaining 10% of the fission energy is emitted to the graphite or other structure elements (Krepel et al., 2005). Therefore, the inner heat sources $S_{T,f}$ and $S_{T,c}$ of the fuel salt and graphite can be calculated as

$$S_{T,f} = 0.9 E_f \cdot \sum_{g=1}^{G} \left(\phi_g \cdot \Sigma_{f,g}\right) \tag{8}$$

$$S_{T,c} = 0.1 E_f \cdot \sum_{g=1}^{G} \left(\phi_g \cdot \Sigma_{f,g}\right) \tag{9}$$

where E_f represents the energy released from each fission reaction.

3.2. Initial and boundary conditions

The theoretical model of the molten salt reactor is conducted during three different transient conditions, which all start from the steady state condition. The steady state calculation model is established by removing the time-dependent items in Eqs. (3)–(7), and introducing the effective multiplication factor shown as

$$\frac{1}{v_1}\nabla \cdot (U\phi_1) = \nabla \cdot D_1 \nabla \phi_1 + \frac{(1-\beta)}{k_{eff}} \cdot \sum_{g=1}^{2} \left(\nu \Sigma_f\right)_g \cdot \phi_g + \sum_{i=1}^{6} \lambda_i \cdot C_i - \phi_1 \cdot \Sigma_{r,1} \tag{10}$$

$$\frac{1}{v_2}\nabla \cdot (U\phi_2) = \nabla \cdot D_2 \nabla \phi_2 + \phi_1 \Sigma_{1\to 2} - \phi_2 \cdot \Sigma_{r,2} \tag{11}$$

$$\nabla \cdot (UC_i) = \frac{\beta_i}{k_{eff}} \cdot \sum_{g=1}^{2} \cdot \left(\nu \Sigma_f\right)_g \cdot \phi_g - \lambda_i \cdot C_i \tag{12}$$

$$\nabla \cdot \left(\rho_f U T_f\right) = \nabla \cdot \frac{K_f}{Cp_f} \nabla T_f + \frac{S_{T,f}}{Cp_f} \tag{13}$$

$$0 = \nabla \cdot \frac{K_c}{Cp_c} \nabla T_c + \frac{S_{T,c}}{Cp_c} \tag{14}$$

The effective multiplication factor k_{eff} is defined as (Xie, 2004)

$$k_{eff}^{(n)} = \frac{\iiint \left[\left(\nu \Sigma_f\right)_1 \cdot \phi_1^{(n)} + \left(\nu \Sigma_f\right)_2 \cdot \phi_2^{(n)}\right] dV}{1/k_{eff}^{(n-1)} \iiint \left[\left(\nu \Sigma_f\right)_1 \cdot \phi_1^{(n-1)} + \left(\nu \Sigma_f\right)_2 \cdot \phi_2^{(n-1)}\right] dV} \tag{15}$$

where the superscripts (n) and $(n-1)$ mean the neutrons of the generation n and $(n-1)$.

The boundary conditions for the fast and thermal fluxes are set as vacuum at the core inlet, outlet, and on the outside surface of the graphite reflector; the symmetric boundary condition is applied for the core axial. For the delayed neutron precursors, the boundary conditions on the outside surfaces of the graphite

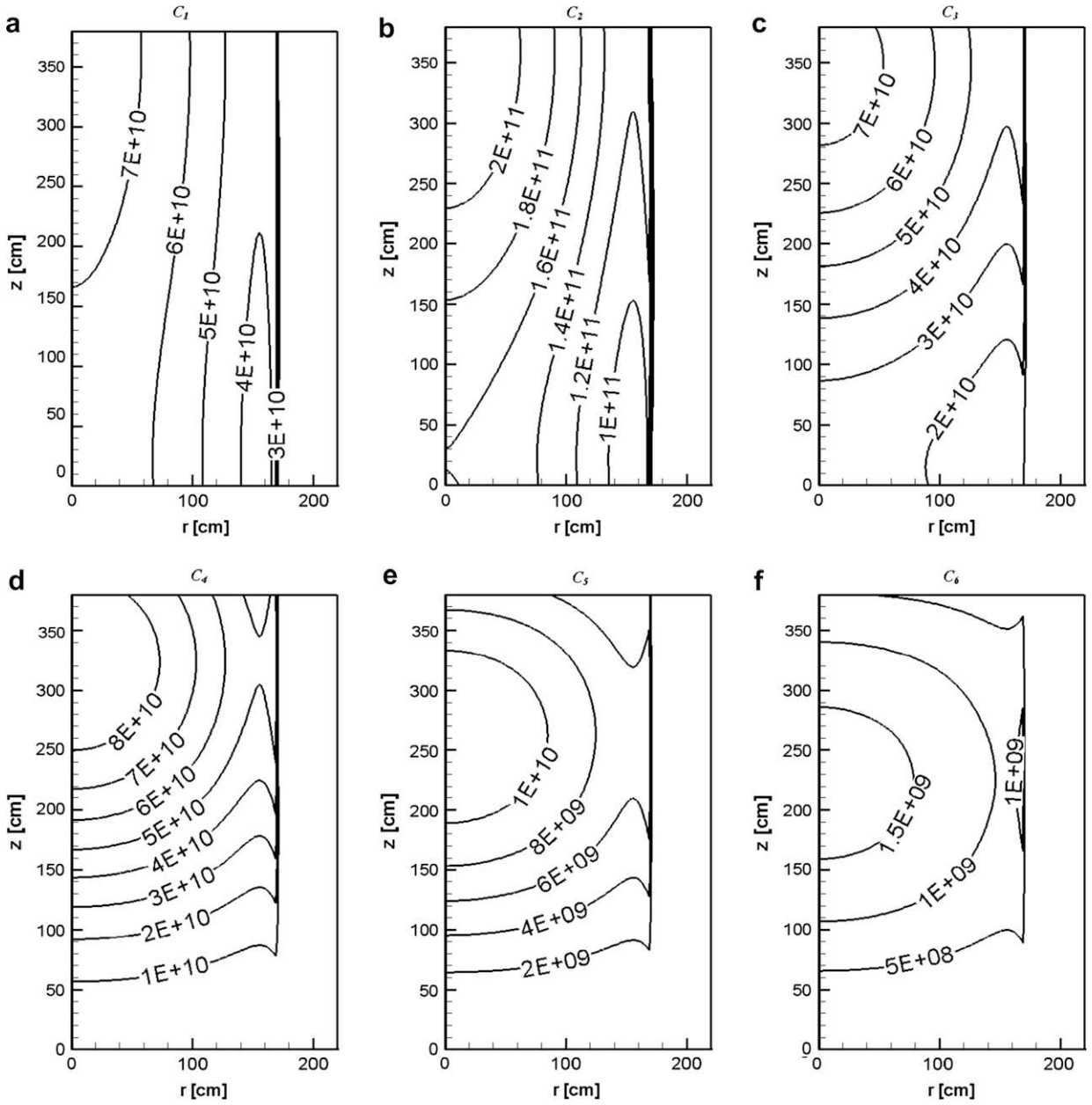

Fig. 11. Distributions of the delayed neutron precursors after the rods drop 0.05 s.

reflector are also set as vacuum condition. However, the precursors can flow out of the core because of their delayed characteristics, the inlet and outlet boundary conditions of which must be given more attention. The precursors outflow of the reactor core with the fuel salt, pass through the external loop, then re-inflow the core bottom. If defining the circulate time of fuel salt in the external loop as τ_{loop}, the re-inflow delayed neutron precursors $C_{i,\text{in}}$ are deduced as

$$C_{i,\text{in}} = C_{i,\text{out}} \cdot \exp\left(-\lambda_i \cdot \tau_{\text{loop}}\right) \tag{16}$$

Eq. (16) is the inlet boundary condition for the delayed neutron precursors. At the outlet a free outflow condition is assumed for the precursors.

The temperature at the core inlet is given as 873 K at the initial steady state condition, and at the outlet, a free outflow condition is assumed. The adiabatic boundary condition is adopted on the outside surfaces of the graphite reflector for the temperature, and the symmetric boundary is used on the core axial.

3.3. Computation of group constants

The group constants in Eqs. (3)–(5) and Eqs. (10)–(12), the diffusion coefficients D_1, D_2, macroscopic fission cross sections $\Sigma_{f,1}$, $\Sigma_{f,2}$, macroscopic removal cross sections $\Sigma_{r,1}$, $\Sigma_{r,2}$, and macroscopic transfer cross section $\Sigma_{1\to 2}$ are needed for the model calculation, and all of the group constants are dependent on the temperature. The WIMSD-IAEA-172 group microscopic cross section library (IAEA, 2007) in this study is used to generate the microscopic cross section database, which is then merged into two-group macroscopic cross sections (group constants) by the code DRAGON (Marleau et al., 1996).

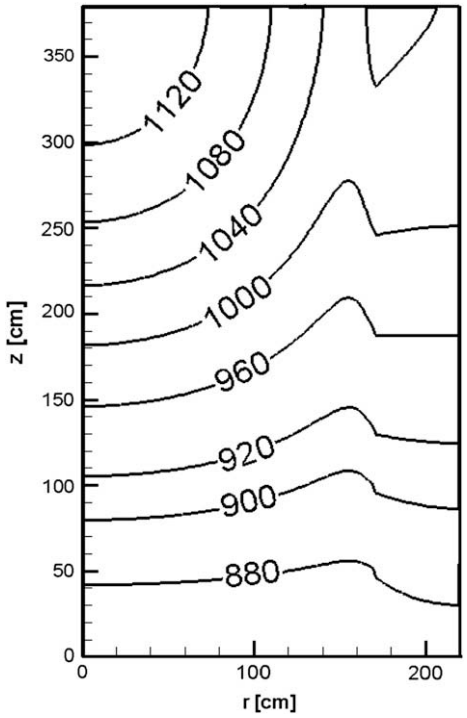

Fig. 12. The temperature distribution after the rods drop 0.05 s.

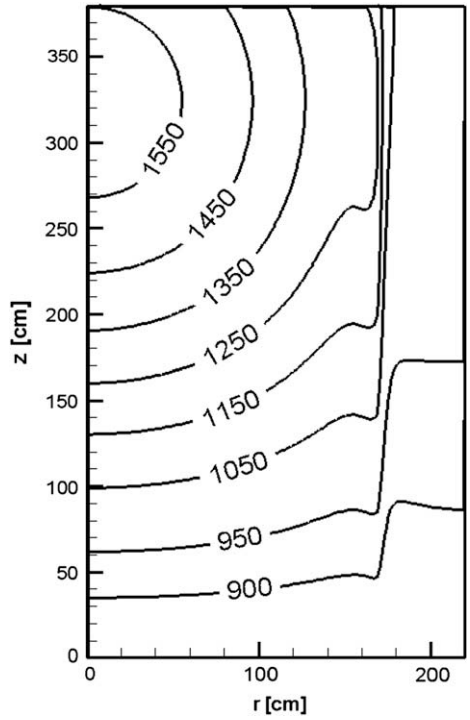

Fig. 14. The temperature distribution after the pump coastdown 20 s.

3.4. Numerical methods

The time-dependent equations (3)–(7) can be written in a unified form

$$\frac{\partial(\rho_X X)}{\partial t} + \nabla\cdot(\rho_X U X) = \nabla\cdot(\Gamma_X \nabla X) + S_X \tag{17}$$

where X represents the calculated variables $\phi_g (g = 1, 2)$, $C_i (i = 1,\ldots,6)$, and T.

If let $t \to \infty$, Eq. (17) is also applicable for the governing Eqs. (10)–(14) under the steady state condition.

Eq. (17) is discretized by the finite volume method to guarantee its conservation characteristics, in which the power law scheme is adopted for the convective and diffusion items while the fully implicit scheme for the time-dependent items. The following discretization equation is obtained

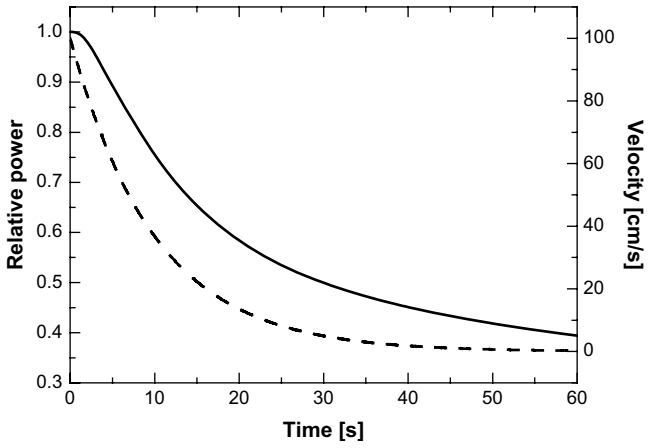

Fig. 13. Behavior of the relative power under the pump coastdown condition.

$$a_P X_P = a_W X_W + a_E X_E + a_N X_N + a_S X_S + b \tag{18}$$

where A_P, A_W, A_E, A_N, and b are the equation coefficients, the expressions of which can be found in the reference Tao (2004); the subscript P represents the main control node, and W, E, N and S are the nodes surrounding the node P.

Applying Eq. (18) for all control nodes, a set of pentadiagonal equations will be built, and the alternating direction implicit TDMA algorithm (Tao, 2004) is adopted to solve it by developing a code. The velocity field used in this study is assumed that only the velocity along the flow direction is considered, which is given as 100 cm s^{-1} under the initial steady state condition.

4. Results and discussion

4.1. Validation of the calculation code

The benchmark TWIGL seed blanket (Liao, 2002) was adopted to validate the code, in which the flow is neglected by assuming velocity equal to zero. Fig. 3 shows the comparison of the calculated results and the benchmark values under two transient conditions. It can be seen that the results calculated by the present code are very well consistent with the benchmark results, which proves that the developed code is valid for the neutron kinetic calculation.

4.2. Sensitivity analysis of grid and time step dependence

The sensitivities of the grid and time step dependence are analyzed under the rods drop condition. Three different uniform grid systems as grid space equal to 1 cm, 2 cm, 5 cm are investigated to validate the solution independency of the grid number. The effective multiplication factor k_{eff} changing with the iteration times under the steady state condition for the three different grid systems is shown in Fig. 4, from which it can be seen that no difference

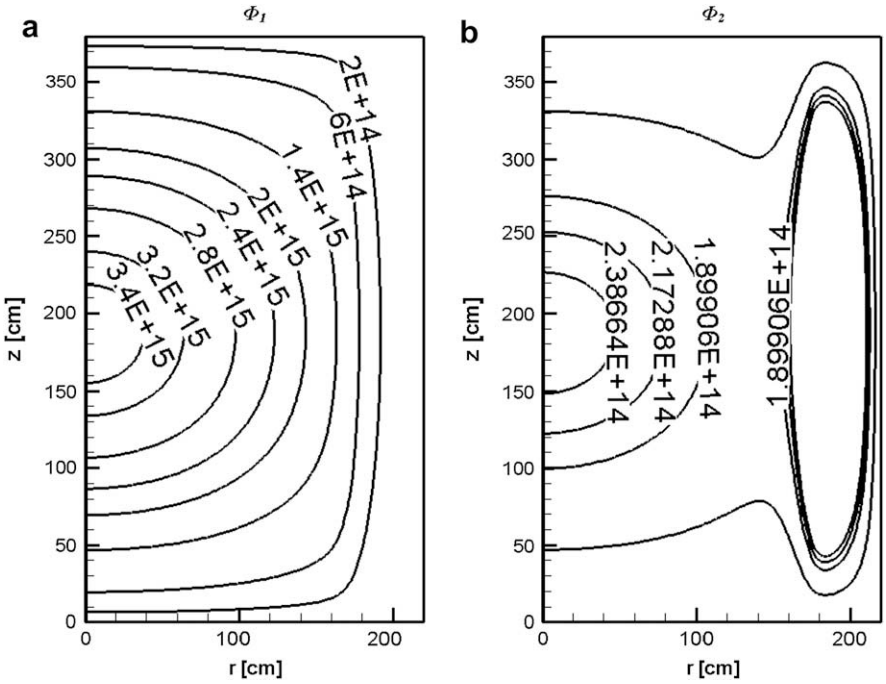

Fig. 15. Distributions of the neutron fluxes after the pump coastdown 20 s.

exists among the convergent k_{eff} obtained from the three different grid systems. Therefore, every one of them can be regarded as grid-independent. The grid space equal to 5 cm is adopted as the final grid system.

The time step must be paid much more attention for the transient problem. Three different time steps of 10^{-3} s, 10^{-4} s and 10^{-5} s are investigated in the numerical calculation. The relative power during the rods drop transient under three different time steps is displayed in Fig. 5. From Fig. 5, it can be seen that the two curves under the time step of 10^{-4} s and 10^{-5} s nearly overlap, and the results under the time step of 10^{-3} s deviate a little from them. Therefore, the time step of 10^{-4} s is used as the final time step in the transient simulation.

4.3. Distributions of the temperature, neutron fluxes and precursors under the steady state condition

Three kinds of transient conditions, the rods drop transient, pump coastdown transient and inlet temperature drop transient, are calculated to research the neutron kinetic characteristics of the molten salt reactor. All of these three transient calculations start from the same initial steady state condition, and the distributions of the temperature, neutron fluxes and the delayed neutron precursors under the initial steady state condition are shown in Figs. 6–8.

Fig. 6 depicts the temperature distribution in the core, which illustrates that the temperature increases along the axial direction, and reaches the maximum 1120 K at the core outlet. Fig. 7(a) and (b) shows the distributions of the fast and thermal neutron fluxes, which are similar with those of a bare reactor, in which the peaks occur in the center region. From Eqs. (10) and (11), it can be found that the velocity of the fuel salt is much smaller than that of the neutron, which means that the convective items in the governing equations of the fast and neutron fluxes can be neglected. Therefore, the fuel salt flow has little effect on the fast and thermal neutron fluxes. In addition, for the thermal neutron flux, there is an increase near the surrounding graphite, that's because the moderation ability of the graphite is strong. Fig. 8 shows the distributions of the delayed neutron precursors under the steady state condition, from which, it can be found that the peaks of the delayed neutron precursors move towards the outlet of the core due to the fuel salt flow influence, and the extent of the motion increases with the decay constants decreasing. Therefore, it could be concluded that the fuel salt flow has little effect on the fast and thermal fluxes under the steady state condition, however, it influences the delayed neutron precursors significantly, especially the ones with small decay constants.

4.4. Rods drop

The first transient presented is the simulation of the pseudo rods drop transient, which is similar with the reactivity inserting accident. In this simulation, rods with 80% Ag–15% In–5% Cd are hypothesized inserting into the center region (rods region) with the radius 60 cm, and the flow in the core is assumed to be not changing. The group constants in the rods region are constants calculated by the code DRAGON as shown in Table 2.

Fig. 9 displays the behavior of the relative power (related to the power under the steady state condition), from which, it can be found that the core power sharply reduces to less than 2% of its original value in 0.02 s after the transient condition occurs, and then decreases very slowly.

When the rods are assumed dropping into the rods region, the absorption cross sections of the fast and thermal neutrons in the region increase sharply, which makes the fast and the thermal fluxes decrease suddenly in that region correspondingly. Fig. 10(a) and (b) displays the changes of the fast and thermal fluxes after the rods drop 0.05 s, from which it can be obviously seen that the values of the fast and thermal fluxes in the rods region decrease sharply, while the higher local fast and thermal fluxes are found to occur in the annular fuel salt region between the rods region and the graphite region. However, the distributions of the delayed neutron precursors change little when the rods drop transient happens (see Fig. 11(a)–(f)), because the life times ($1/\lambda_i$) of the delayed neutron precursors are so long that the precursors hardly

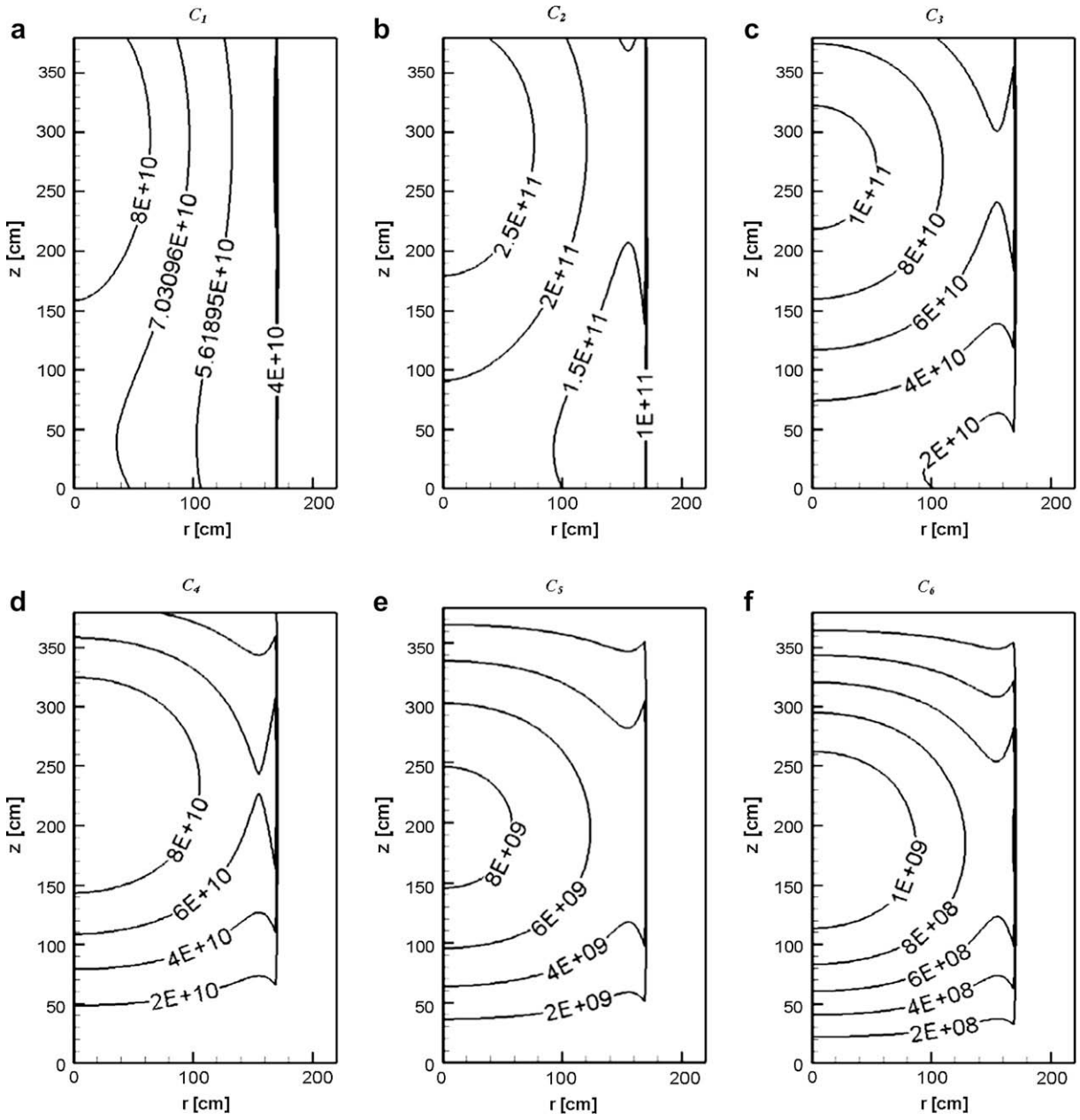

Fig. 16. Distributions of the delayed neutron precursors after the pump coastdown 20 s.

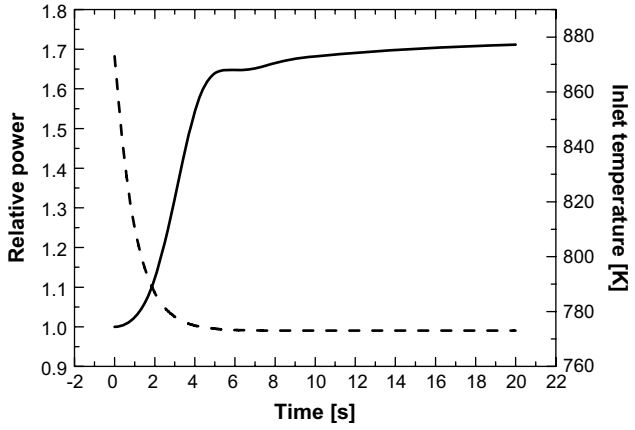

Fig. 17. Behavior of the relative power under the inlet temperature drop condition.

decay in 0.05 s. Fig. 12 shows the temperature distribution in the core, comparing with that under the steady state condition, little differences can be found. The reason is that the responding of the heat transfer to the transient condition is much slower than that of the neutron fluxes. From the pseudo rods drop transient, it can be concluded that the fast and thermal neutron fluxes respond to the reactivity inserting faster than the temperature and the delayed neutron precursors do.

4.5. Pump coastdown

The pump coastdown accident is simulated by reducing the velocity in the core according to the exponential law,

$$u = u_0 e^{-\lambda_{\text{pump}} \cdot t} \tag{19}$$

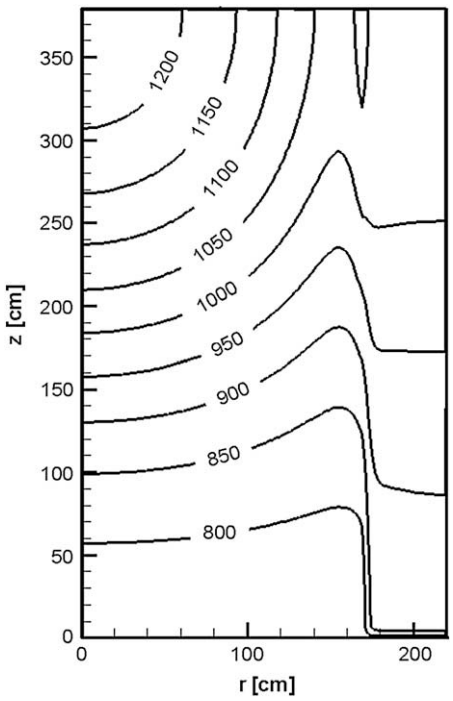

Fig. 18. The temperature distribution after the inlet temperature drop 10 s.

where u_0 is the initial velocity, and λ_{pump} is the coastdown coefficient of the pump, which is assumed as 0.1 s in the present study. The velocity in the core varying with the time is shown in Fig. 13 by the dashed line.

The behavior of the relative power under the pump coastdown condition is shown in Fig. 13 represented by the solid line, from which it can be found that the relative power decreasing with time is approximately exponential, which reflects the positive feedback effect of the fuel salt flow on the reactivity. In fact, the velocity reduction leads to the temperature increasing in the core, which is correlative with the group constants in the neutron kinetic model. Therefore, the relative power decreases during the pump coastdown transient because of the negative feedback effect of the temperature on the reactivity. Furthermore, from Fig. 13, it can also be found that the relative power changes very small in the beginning phase until 2 s, that's because the temperature response is slower, which has been shown in the rods drop transient.

After the pump coastdown 20 s, the velocity reduces to about 13.5 cm s^{-1}, at this time, the distributions of the temperature, neutron fluxes and delayed neutron precursors are represented in Figs. 14–16. From Fig. 14, it can be obviously seen that the maximum temperature at the core outlet reaches 1550 K, which is about 430 K higher than that under the initial steady state condition due to the velocity decrease. Because of the positive feedback effect of the fuel salt flow on the reactivity, the values of both the fast and thermal neutron fluxes decrease as shown in Fig. 15(a) and (b), however, the distribution patterns are similar with those under the steady state condition. From Fig. 16, it can be found that the extents of the delayed neutron precursors removing towards the core outlet decrease comparing with those under the initial steady state condition, and the influences of the flow changing on the delayed neutron precursors increase with the decay constants of the precursors.

4.6. Inlet temperature drop

The temperature drop at the inlet is also conducted. The reduction law of the inlet temperature is assumed as the exponential as shown below

$$T_{in} = T_{in,0} - 100\left(1 - e^{-0.1\cdot t}\right) \tag{20}$$

where T_{in} denotes the inlet temperature, and $T_{in,0}$ is the inlet temperature under the steady state condition.

The solid line in Fig. 17 depicts the behavior of the relative power under the inlet temperature drop condition. The relative power

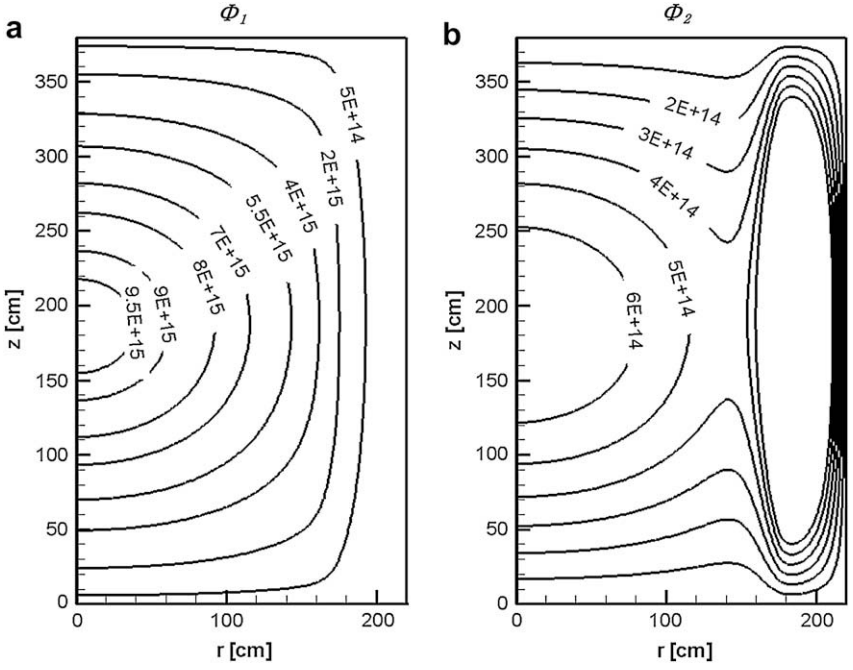

Fig. 19. Distributions of the neutron fluxes after the inlet temperature drop 10 s.

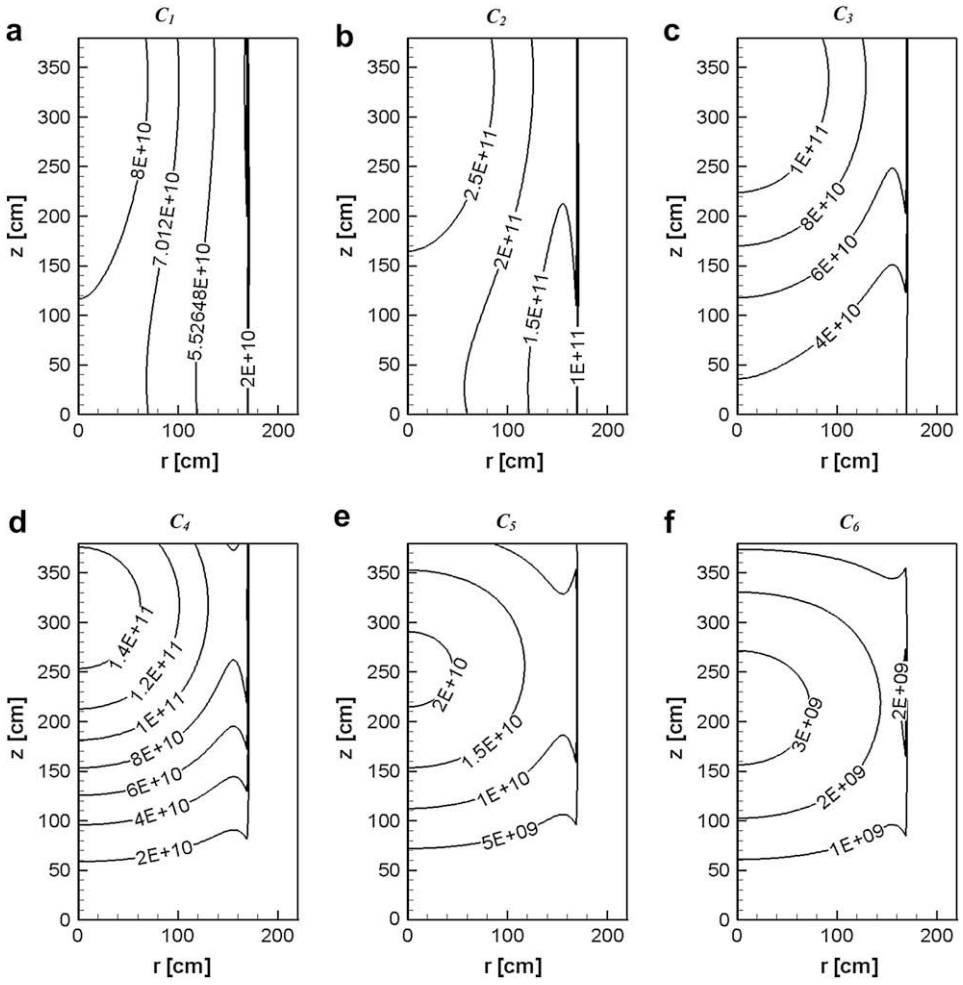

Fig. 20. Distributions of the neutron fluxes after the inlet temperature drop 10 s.

increases rapidly to 1.64 in 5 s, and then increases very slowly, which is corresponding to the inlet temperature reduction (shown in Fig. 17 represented by the dashed line). In addition, the characteristics of the relative power varying with time reflect the negative feedback effect of the inlet temperature on the reactivity.

Figs. 18–20 display the distributions of the temperature, neutron fluxes and delayed neutron precursors after 10 s of the inlet temperature drop. The negative feedback of the temperature on the reactivity leads to the power increasing, which results in the temperature in the core rise. From Fig. 18, it can be found that the maximum temperature in the core is 1200 K, which is a little higher than that under the steady state condition. Fig. 19(a) and (b) illustrates the distributions of the fast and thermal neutron fluxes, the values of which increase a little comparing with those under the steady state condition, though the distribution patterns are similar. The distribution patterns of the delayed neutron precursors (see Fig. 20(a)–(f)) are nearly the same with those under the steady state condition because the flow condition remains unchanged. However, the values of the delayed neutron precursors after 10 s of the inlet temperature drop are larger due to negative reactivity feedback, comparing with those under the steady state condition.

5. Conclusions

In the present research, the theoretical model of the neutron kinetics considering the fuel salt flow for the molten salt reactor is established and calculated by developing a numerical code. A heat transfer model is also found to consider the temperature feedback on the neutron kinetics, in which the group constants dependent on the temperature are calculated by the code DRAGON. Three transient conditions including the rods drop, pump coastdown and the inlet temperature drop conditions are simulated to analyze the neutron kinetic characteristics of the molten salt reactor.

Main results obtained in this research show that the fuel salt flow has little effect on the fast and thermal fluxes under the steady state condition. However, it influences the delayed neutron precursors significantly, especially the ones with small decay constants. From the transient calculation, it can be found that the relative power rapidly decreases during the rods drop transient, and the fast and thermal neutron fluxes respond to the transient quickly, however, the temperature and the delayed neutron precursors respond slowly; the relative power also decreases exponentially when the pump coastdown decays exponentially. In addition, the flow change has a greater influence on the delayed neutron precursors with larger decay constants; the inlet temperature drop leads to the negative reactivity feedback on the neutron kinetics in the molten salt reactor.

Acknowledgements

This work is carried out under the financial support of the National Natural Science Foundation of China (Grant No.

10575079). And the authors also wish to acknowledge Dr. S. Wang of Institute for Nuclear and Energy Technologies (IKET) of FZK for his valuable supports and comments.

References

Dulla, S., Ravetto, P., Rostagno, M.M., 2003. Neutron kinetics of fluid-fuel systems by the quasi-static method. Ann. Nucl. Energy 31, 1709.

IAEA, 2007. The basic nuclear data file is available on-line at the website: http://www-nds.iaea.org.

Ignatiev, V., Feynberg, O., Myasnikov, A., 16–20 November 2003. Neutronic properties and possible fuel cycle of a molten salt transmuter. In: Proceedings of the 2003 ANS/ENS International Winter Meeting (GLOBAL 2003). Hyatt Regency, New Orleans, LA, USA.

Krepel, J., Grundmann, U., Rohde, U., 2005. DYN1D-MSR dynamics code for molten salt reactors. Ann. Nucl. Energy 32, 1799.

Krepel, J., Grundmann, U., Rohde, U., 2007. DYN3D-MSR spatial dynamics code for molten salt reactors. Ann. Nucl. Energy 34, 449.

Lapenta, G., Mattioda, F., Ravetto, P., 2000. Point kinetic model for fluid fuel systems. Ann. Nucl. Energy 28, 1759.

Liao, C.K., 2002. Steady on Numerical Method for Three Dimensional Nodal Space-Time Neutron Kinetic Equations and Coupled Neutronic/Thermal-Hydraulic Core Transient Analysis. Xi'an Jiaotong University.

Marleau, G., Hebert, A., Roy, R., 1996. A User's Guide for DRAGON. Technical Report, Report IGE-174. Ecole Polytechnique de Montreal, Canada.

Mitachi, K., Yamana, Y., Suzuki, T., 1995. Neutronic Examination on Plutonium Transmutation by a Small Molten-Salt Fission Power Station Technical Report [R], IAEA-TECDOC-840.

Most Project, 2004. Molten salt reactor technology phase 1. In: Proceedings of the 5th Framework Programme of European Commission, October 2001–December 2003.

Nicolino, C., Lapenta, G., Dulla, S., 2008. Coupled dynamics in the physics of molten salt reactors. Ann. Nucl. Energy 35, 314.

Tao, W.Q., 2004. Numerical Heat Transfer, second ed. Xi'an Jiaotong University Press, Xi'an.

Xie, Z.S., 2004. Nuclear Physics Analysis. Xi'an Jiaotong University Press, Xi'an.

Yamamoto, T., Mitachi, K., Ikeuchi, K., 2006. Transient characteristics of small molten salt reactor during blockage accident. Heat Transfer Asian Res. 35, 434.